JACS
JOURNAL OF THE AMERICAN CHEMICAL SOCIETY
Article
pubs.acs.org/JACS

A De Novo Designed 2[4Fe-4S] Ferredoxin Mimic Mediates Electron Transfer

Anindya Roy,[†,§,⊥] Dayn Joseph Sommer,[†,§] Robert Arthur Schmitz,[†] Chelsea Lynn Brown,[†] Devens Gust,[†] Andrei Astashkin,[‡] and Giovanna Ghirlanda*[,†]

[†]Department of Chemistry and Biochemistry, Arizona State University, Tempe, Arizona 85287-1604, United States
[‡]Department of Chemistry and Biochemistry, University of Arizona, Tucson, Arizona 85721, United States

Supporting Information

ABSTRACT: [Fe-S] clusters, nature's modular electron transfer units, are often arranged in chains that support long-range electron transfer. Despite considerable interest, the design of biomimetic artificial systems emulating multicluster-binding proteins, with the final goal of integrating them in man-made oxidoreductases, remains elusive. Here, we report a novel bis-[4Fe-4S] cluster binding protein, DSD-Fdm, in which the two clusters are positioned within a distance of 12 Å, compatible with the electronic coupling necessary for efficient electron transfer. The design exploits the structural repeat of coiled coils as well as the symmetry of the starting scaffold, a homodimeric helical protein (DSD). In total, eight hydrophobic residues in the core of DSD were replaced by eight cysteine residues that serve as ligands to the [4Fe-4S] clusters. Incorporation of two [4Fe-4S] clusters proceeds with high yield. The two [4Fe-4S] clusters are located in the hydrophobic core of the helical bundle as characterized by various biophysical techniques. The secondary structure of the apo and holo proteins is conserved; further, the incorporation of clusters results in stabilization of the protein with respect to chemical denaturation. Most importantly, this de novo designed protein can mimic the function of natural ferredoxins: we show here that reduced DSD-Fdm transfers electrons to cytochrome *c*, thus generating the reduced cyt *c* stoichiometrically.

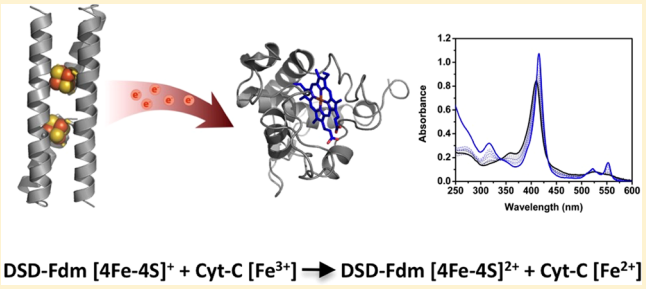

INTRODUCTION

Ferredoxins are nature's electron transfer modules, supporting crucial processes such as photosynthesis and respiration.[1−5] The so-called bacterial type consists of small proteins containing two cubane-like [4Fe-4S] clusters within sequences of 50−60 amino acids. Each cluster is coordinated by four cysteine residues and ensconced in one of two pseudosymmetric domains thought to derive from a gene duplication event.[4,6] Ferredoxins function as one-electron shuttles and couple oxidation of several substrates with reduction of cofactors or final acceptors such as H^+ or $NADP^+$.[2,7−9] The ferredoxin fold has also been coopted as a separate subunit (e.g., PsaC) or as an integral domain within complex enzymes, such as photosystem I and the hydrogenases.[10−16] In these redox proteins, chains of [4Fe-4S] clusters transfer electrons produced or consumed at a buried active site to the protein surface, allowing interaction with soluble partners. To optimize the rates of electron transfer, the clusters are typically separated by up to 12−14 Å.

A substantial amount of work in the field of *de novo* design has sought to incorporate the clusters into peptide-based model systems, to elucidate the properties of the natural cluster environment, and eventually to include these model peptides in engineered redox enzymes.[7,10,17−24] Most of these peptides, however, have been designed to bind a single electronically isolated cluster, which limits their usefulness as electron conduits *in vitro*. To address this problem, we have recently developed a general method to design bis-[4Fe-4S] cluster binding peptides by exploiting the symmetry of coiled coils. Using this approach, we have shown that two [4Fe-4S] clusters can be incorporated inside the hydrophobic core of a three-helix bundle.[25] However, the distance separating the two clusters in our prototype was 36 Å, which did not provide a useful platform for studying efficient electron transfer. Here, we present a second generation design, DSD-Fdm, in which the two clusters are located within 12 Å of each other, a biologically relevant distance for effective electron transfer. The redox potential of DSD-Fdm falls within the range observed for natural ferredoxins, suggesting that this artificial protein could engage in electron transfer with external redox active species. We show that DSD-Fdm is capable of transferring electrons to cytochrome *c* in a stoichiometric manner. Further, DSD-Fdm undergoes energy transfer in the presence of a photosensitizer, suggesting a possible use in solar fuel cell applications.

Received: October 16, 2014
Published: November 20, 2014

   dx.doi.org/10.1021/ja510621e | J. Am. Chem. Soc. 2014, 136, 17343−17349

METHODS

Peptide Synthesis and Purification. All peptides were synthesized by automated microwave-assisted solid phase peptide synthesis on a Liberty instrument (CEM). The synthesis was carried out using standard Fmoc protection procedures. Briefly, Rink amide resin was doubly deprotected using 0.1 M hydroxybenzotriazole (HOBt) in a solution of 20% piperidine in DMF. Amino acid couplings were achieved using appropriate amounts of 0.45 M *N*,*N*,*N*′,*N*′-tetramethyl-*O*-(1*H*-benzotriazol-1-yl)uronium hexafluorophosphate (HBTU) in DMF, 2 M ethyl-diisopropylamine (DIEA) in *N*-methyl-2-pyrrolidone (NMP), and 0.2 M fluorenylmethyloxycarbonyl (Fmoc) protected amino acid (Novabiochem), followed by irradiation with microwaves to pre-established temperatures according to CEM protocols. Peptides were acetylated at the N-terminus via addition of acetic anhydride under coupling conditions. The peptides were cleaved from the resin using 94% trifluoroacetic acid (TFA), 2.5% H_2O, 2.5% 1,2-ethanedithiol (EDT), and 1% triisopropylsilane (TIS) for 3 h. The solution was then evaporated under a stream of N_2, and the peptide was precipitated with cold ether. Crude lyophilized peptides were purified using preparatory-scale high performance liquid chromatography (HPLC) on a C18 reverse-phase column, with a linear gradient of solvent A (99.9% water with 0.1% TFA) and solvent B (95% acetonitrile, 4.9% water, and 0.1% TFA) at a flow rate of 10 mL/min. Peptide identity was confirmed by matrix-assisted laser desorption ionization time-of-flight mass spectrometry (MALDI-TOF-MS); peptides were >99% pure as assessed by C18 analytical HPLC.

Cluster Incorporation and Quantification. Iron−sulfur clusters were incorporated into peptide variants by adapting well-established methodologies.[18,26] All reactions were performed in an anaerobic chamber (Coy Scientific), with a 95% N_2 and 5% H_2 environment. To a solution of 150 μM peptide in 100 mM Tris-HCl, pH 8.5, the following reagents were added sequentially at 20 min intervals to a final concentration: 0.8% (v/v) β-mercaptoethanol, 3 mM ferric chloride ($FeCl_3$), and 3 mM sodium sulfide (Na_2S). The mixture was incubated overnight at 4 °C. The resulting dark brown solution was subjected to desalting with a PD10 G25 column (GE Healthcare) that was pre-equilibrated with 100 mM Tris at pH 7.5 to obtain the holo protein.

Cluster Quantification. Cluster incorporation was assessed quantitatively by measuring independently the concentration of iron and of peptide in identical samples.[25] DSD-Fdm samples were further purified using anion exchange chromatography on a Q-Sepharose FF column (GE Healthcare), using 100 mM Tris at pH 8.5 as equilibration buffer and 100 mM NaCl, 100 mM Tris at pH 8.5 as elution buffer. The DSD-Fdm samples were split in two portions: one was used to measure peptide concentration (Bradford assay), and the second was used to determine iron concentration (ferrozine assay).[27,28] EPR spin quantification was used to assess the amount of reduced clusters in concentrated EPR samples. The double integral of the CW EPR spectrum of $[4Fe\text{-}4S]^+$ recorded at 7 K was compared with the spectrum of 5 mM Cu(II) nitrate recorded at 21 K (at lower temperatures, the Cu(II) EPR signal saturated even at the lowest accessible MW power of 0.2 μW). The estimated concentration of $[4Fe\text{-}4S]^+$ was then compared with the DSD-Fdm protein concentration evaluated by Bradford assay.

Gel Filtration. Size exclusion chromatography was performed on a G-25 gel filtration column fit to an Agilent Technologies 1260 Insight FPLC system. The column was pre-equilibrated in 100 mM Tris-HCl, pH 7.5, and 200 μL of 150 μM apo or holo peptide were used for each injection. The apo peptide was pretreated with tris(2-carboxyethyl)-phosphine (TCEP) for 30 min before injection to reduce any disulfides resulting from air oxidation.

Circular Dichroism Spectroscopy. Spectra were recorded on a JASCO J-815 spectropolarimeter in the range of 190−260 nm. Data were recorded every 1 nm and averaged over three scans. The concentrations of apo and holo peptides were kept at 50 μM in 100 mM Tris, pH 7.5, while the measurements of the apo peptide were carried out in the presence of an excess of TCEP. Holo peptide was measured under anaerobic conditions in an airtight CD cuvette. Chemical denaturation titrations were carried out through addition of an 8 M stock solution of guanidinium-HCl (Gdn·HCl), followed by mixing and incubation for 5 min to allow for equilibration. Holo peptide was titrated under anaerobic conditions. Spectra were normalized to protein concentration in the sample and converted to fraction folded relative to the apo or holo protein signal, which lacked Gdn·HCl.

Electron Paramagnetic Resonance Spectroscopy. Holo protein obtained from PD10 desalting was concentrated in a 3000 MWCO centrifuge concentrator to approximately 1 mM peptide concentration. Reduced samples were prepared by addition of 100 mM sodium dithionite in 1 M glycine buffer, pH 10, to a final concentration of 20 mM dithionite. EPR samples were prepared by addition of 10% (v/v) glycerol as a cryoprotectant and placed in quartz EPR tubes, after which the samples were flash frozen and stored under liquid N_2 until measurements. Continuous wave (CW) EPR experiments were carried out on a X-band EPR spectrometer Elexsys E500 (Bruker) equipped with the ESR900 flow cryostat (Oxford Instruments).

Synthesis of Water-Soluble Porphyrin Analogue. The 5,10,15,20-tetrakis(4-diethyl 2-benzylmalonate) porphyrin was synthesized following published procedures for related compounds.[7,29] Zinc insertion was achieved using $Zn(O_2CCH_3)_2(H_2O)_2$ in THF for 12 h at 60 °C by modifying a literature procedure (Figure S1, Supporting Information),[30−32] and the esters were cleaved as reported for related compounds.[10,18,33,34] The resulting water-soluble, malonate-functionalized porphyrin was characterized by mass spectrometry and NMR in D_2O (Figures S2 and S3, Supporting Information).

Transient Absorption Spectroscopy. Nanosecond transient absorption measurements were performed on a flash photolysis apparatus using a pulsed laser source and a pump−probe optical setup. The samples contained 10 mM Tris-HCl at pH 7.5 with 30 μM holo or apo peptide in a 1 cm fluorescence cuvette. Malonate-porphyrin was added to a final absorbance of 0.25 at the first Q-band (560 nm). Excitation was provided by an optical parametric oscillator pumped by the third harmonic (352 nm) of a Nd:YAG laser (Ekspla NT 342B). The pulse width was 4−5 ns, and the repetition rate was 10 Hz. The signal was detected by a Proteus spectrometer (Ultrafast Systems). The instrument response function was 4−5 ns. Transient data analysis was carried out using the in-house program ASUFIT. Simple exponentials were fit one wavelength at a time.

Cytochrome c_{550} Reduction Assay. DSD-Fdm was reduced via slow addition of dithionite, monitoring the loss of signal at 410 nm. Once the absorption at 410 nm had stabilized and a slight dithionite signal had arisen at 300 nm, the holo peptide was subjected to two successive PD10 columns to exclude any unreacted dithionite. The first 1.5 mL of the total 3.5 mL elution volume was concentrated to a protein concentration of 300 μM. The reduced DSD-Fdm was added in 1 μL increments to 500 μL of a solution of cytochrome c_{550} isolated from *Thermosynechococcus elongatus* (7 μM protein concentration as assayed by absorbance at 550 nm, ε_{550} = 21000 M^{-1} cm^{-1}). After each addition, UV−vis spectra were obtained with an Ocean Optics USB4000 detector fitted with a USB-ISS-UV-Vis light source. Data were fit by a linear regression model before and after saturation in order to determine the mole equivalents required to obtain full reduction of the cytochrome c_{550} heme cofactor.

RESULTS AND DISCUSSION

Protein Design and Synthesis. We used the heptad repeat pattern of coiled coils, which is reflected in a regular structural motif, to design two [4Fe4S] binding sites into the core of DSD-Fdm starting from DSD-bis[4Fe4S].[25,26] Each site was translated by one heptad toward the center of DSD along the longitudinal axis (PDB code 1G6U) by moving the two cysteine side chains arranged at the *i*, *i*+3 positions within the same helix. Locations for the two remaining cysteines, one per helix, in positions compatible with chelating the cluster were determined by manually docking a [4Fe-4S] cluster binding site

dx.doi.org/10.1021/ja510621e | J. Am. Chem. Soc. 2014, 136, 17343−17349

from *Thermotoga maritima* (PDB ID 2G36)[1−5] inside the core (Figure 1). Taking into account the pseudo-2-fold symmetry of

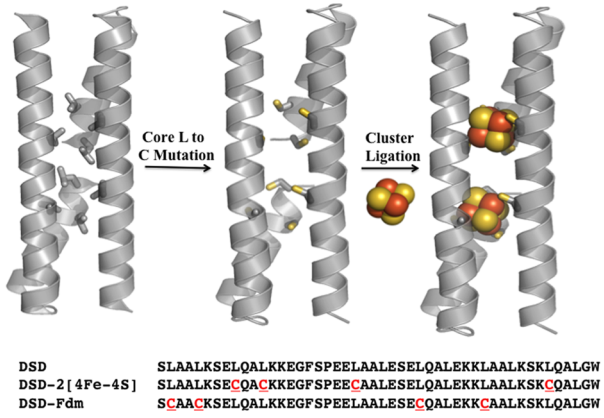

Figure 1. Design strategy for DSD-Fdm (top panel) and sequences of DSD, DSD-2[4Fe4S], and DSD-Fdm (bottom panel).

DSD, we replicated the site onto the other half of DSD by inserting appropriate mutations into the peptide sequence. DSD-Fdm thus incorporates two [4Fe-4S] clusters in the hydrophobic core at a distance of 12 Å, as measured between their centers, in an arrangement reminiscent of the symmetry observed in the natural ferredoxin fold. Mutation of eight core leucine side chains to cysteines causes the formation of a 62 $Å^3$ polar cavity within the core of the apo peptide, which is completely filled upon incorporation of the cluster (Figure 1).[4,6]

Cluster Incorporation. The [4Fe-4S] clusters were formed and incorporated *in situ* from inorganic precursors and mercaptoethanol using established protocols,[2,7−9] and holo DSD-Fdm was purified by gel filtration chromatography.

The UV−vis spectrum of DSD-Fdm shows a broad feature with maxima at 415 and 360 nm, characteristic of sulfur to iron charge transfer excitations in $[4Fe\text{-}4S]^{2+}$ clusters; the absorbance at 415 nm was reduced to below 50% of its initial value upon reduction to $[4Fe\text{-}4S]^{+}$ (Figure 2) with dithionite. This behavior is typical of cuboidal [4Fe-4S] clusters.[10−16] The position of the bands, red-shifted compared with inorganic [4Fe-4S] clusters, suggests that the clusters are surrounded by a hydrophobic environment.[7,10,17−24]

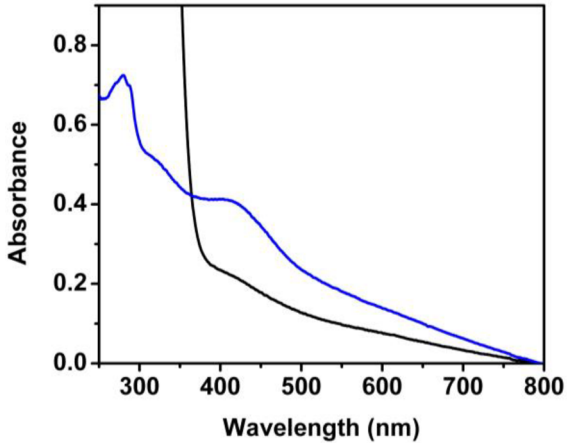

Figure 2. UV−vis spectra of holo DSD-Fdm before (black trace) and after (blue trace) dithionite reduction.

We investigated the oligomeric state of apo and holo DSD-Fdm by analytical ultracentrifugation and size exclusion chromatography. When analyzed by gel filtration, both apo and holo DSD-Fdm elute at comparable volumes of elution buffer, which is consistent with a single species with the apparent molecular mass of a dimer (Figure S4, Supporting Information). The elution profiles of the holo DSD-Fdm monitored at 220, 280, and 410 nm are identical, indicating the presence of the [4Fe-4S] cluster in the dimer. Analytical ultracentrifugation of the apo DSD-Fdm at ∼100 μM loading concentration reveals an apparent molecular weight in solution of approximately 13.3 kDa, consistent with a dimeric form in solution (Figure S5, Supporting Information), confirming the results of the size exclusion chromatography.

We evaluated the level of cluster incorporation in the dimer by independently assessing Fe and protein concentrations as described in Methods. We found that the ratio of iron per monomer is 4.3 ± 0.9, corresponding to two [4Fe-4S] clusters per dimer. These data indicate that incorporation is approximately 100%.

Protein Structure and Stability. We investigated the secondary structure of both apo and holo DSD-Fdm using far-UV circular dichroism (CD) spectroscopy. The spectra of each of the two proteins are similar to that of the parent peptide and display two minima centered at 208 and 222 nm, indicative of helical structures (Figure S6, Supporting Information). Cluster incorporation is well tolerated by the peptide, which is reflected by the similar molar ellipticity value of the holo peptide compared with the apo peptide.

To assess the effect of mutations on the DSD framework, we measured the stability of the apo and holo peptide toward chemical denaturation by monitoring the loss of secondary structure as a function of increasing concentration of a chaotropic agent, guanidine hydrochloride (Gdn·HCl). The denaturation curves in Figure 3 report fraction folded, as

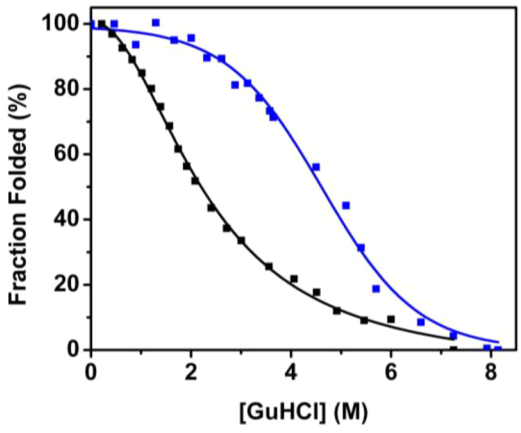

Figure 3. Chemical denaturation profile of 50 μM apo and holo DSD-Fdm monitored by CD at 222 nm. The midpoint of the transition is at 2.1 M Gdn·HCl (black line) for the apo peptide and at 4.4 M Gdn·HCl (blue line) for holo DSD-Fdm.

monitored at 222 nm, versus denaturant concentration for each peptide, showing that holo DSD-Fdm is significantly more stable to chemical denaturants than is the apo version. The midpoint of denaturation for the apo peptide is at 2.1 M Gdn·HCl, while for the holo DSD-Fdm, it is at 4.4 M Gdn·HCl. This behavior mirrors what is observed for DSD-bis[4Fe-4S], for which a large increase in stability resulted from the cluster

dx.doi.org/10.1021/ja510621e | J. Am. Chem. Soc. 2014, 136, 17343−17349

incorporation.[25] The starting scaffold for both constructs, DSD, is exceptionally stable to thermal and chemical denaturation.[18,26] In both DSD-bis[4Fe-4S] and DSD-Fdm, substituting hydrophobic leucine residues in the core with polar, smaller cysteines results in the formation of a polar cavity, which in the case of DSD-Fdm has a volume of 62 Å^3. This volume is compatible with the dimensions of a [4Fe-4S] cluster; when modeled in the peptide core, the [4Fe-4S] cluster completely fills the cavity, thus restoring a well-packed core.

EPR Spectroscopy and Redox Properties of the Cluster. The electronic properties of holo DSD-Fdm were explored by CW EPR spectroscopy. As expected, *in vitro* reconstitution of the iron−sulfur cluster into the designed protein results in formation of an EPR silent $[4Fe\text{-}4S]^{2+}$ resting state. Upon dithionite reduction, an EPR signal corresponding to intact $[4Fe\text{-}4S]^{+}$ clusters arises, with typical principal *g*-values of 1.89, 1.94, and 2.06, and an isotropic *g*-value of about 1.96 (Figure 4). The temperature dependence of this signal is similar

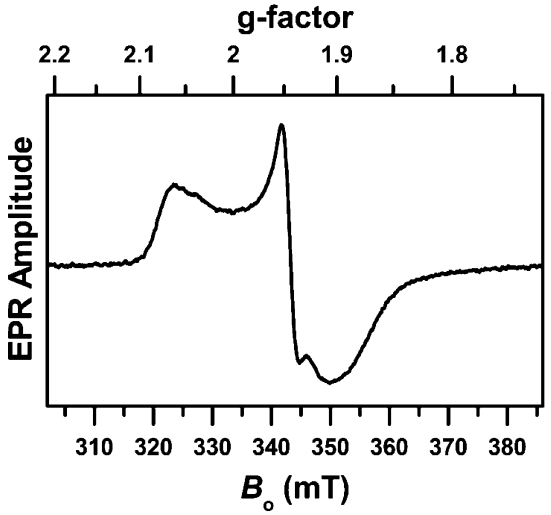

Figure 4. CW EPR spectrum of dithionite-reduced holo DSD-Fdm. Experimental conditions: microwave frequency, 9.337 GHz; microwave power, 20 mW; field modulation amplitude, 0.5 mT; temperature, 12 K.

(if not identical) to that obtained earlier for DSD-bis[4Fe-4S] and indicative of the presence of low-lying (~60 K) excited states (Figure S7, Supporting Information). The spin quantification of this signal and the comparison of the spin count with the protein concentration reveals a yield of reduced cluster per dimer of DSD-Fdm close to 0.6, similar to what has been observed for DSD-bis[4Fe-4S].[25] This value contrasts with complete cluster incorporation yields calculated by iron quantification based on resting state (i.e., oxidized) samples. The discrepancy is caused by difficulties in achieving complete reduction of the cluster in concentrated samples.

Ferredoxin-type proteins containing two $[4Fe\text{-}4S]^{1+}$ within 10−15 Å of each other sometimes exhibit features in the EPR spectra attributable to a spin−spin interaction between the clusters.[27,28] Despite repeated attempts, these features were not observed in the spectra of DSD-Fdm. However, the lack of cluster interaction effects in the CW EPR spectra of dicluster ferredoxins is relatively common, for two main reasons.[7,29] First, the magnitude of the dipole and exchange interactions between two clusters strongly depends on their relative orientation, because of the mixed valence nature of the clusters.[30−32] For example, the dipole interaction constant estimated for DSD-Fdm as a function of the relative orientation of the clusters can be anywhere between ~300 and 25 MHz (in magnetic field units, ~11 and <1 mT, respectively) or distributed within these limits. The smaller of these couplings would probably not be detectable because it is much smaller even than the EPR line width at the intermediate turning point (>3 mT). The larger of these couplings could in principle be resolvable, but the relatively flexible nature of DSD-Fdm may result in a significant broadening and the lack of pronounced features in the EPR spectrum of the pair. The second reason, which compounds the first one, is the relatively low yield of reduced cluster.

The redox properties of DSD-Fdm were probed using cyclic voltammetry (CV). Solution CV experiments showed no observable redox processes in the range from 0 to −1 V vs SHE, presumably because of the absence of interaction between the electrode surface and the electroactive species. Addition of 3.5 mM neomycin, which is known to stabilize and enhance the interaction of ferredoxin type proteins with electrode surfaces, resulted in the observation of a quasi-reversible process with cathodic and anodic waves centered around −0.438 and −0.521 V vs SHE, respectively (Figure 5). We estimated a redox

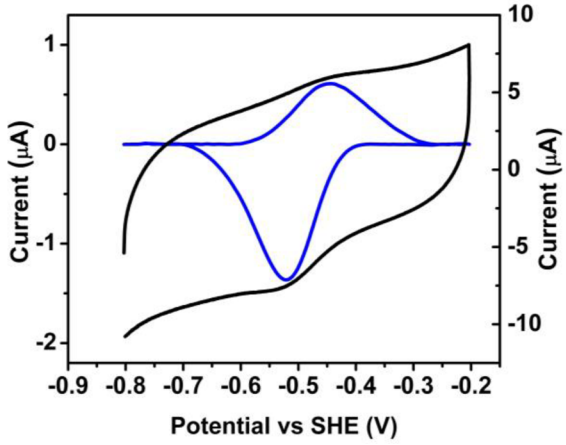

Figure 5. Cyclic voltammogram of DSD-Fdm in a 3.5 mM neomycin, 100 mM Tris, 100 mM sodium chloride, pH 7.5, solution at 100 mV/s scan rate with a Ag/AgCl reference electrode, glassy carbon working electrode, and platinum mesh counter electrode.

potential of −0.479 V vs SHE, consistent with the presence of a $[4Fe\text{-}4S]^{2+/1+}$ couple. This value falls within the window expected for low potential [4Fe-4S] clusters in proteins and is very close to those observed for the PsaC subunit of photosystem I.[10,18,33,34]

Electron Transfer Properties of DSD-Fdm. Because the redox potential of DSD-Fdm is comparable to that of natural ferredoxins, we tested the ability of DSD-Fdm to transfer an electron to a natural protein, oxidized cytochrome *c*. DSD-Fdm was reduced by sequential addition of sodium dithionite, monitoring the loss of absorbance at 410 nm, and stopping addition as soon as the signal stabilized.

The reduced peptide was further purified to remove all excess dithionite and titrated into an air-oxidized sample of *Thermosynechococcus elongatus* cytochrome c_{550}, while monitoring the reaction by UV−vis spectroscopy. We observed shifts of the Soret band (410 to 415 nm) and of the Q-bands (526 to 520 and 550 nm) that indicate reduction of the protein-bound

dx.doi.org/10.1021/ja510621e | J. Am. Chem. Soc. 2014, 136, 17343−17349

heme (Figure 6). A plot of the change of absorbance at 415 nm as a function of molar equivalents of holo DSD-Fdm reveals

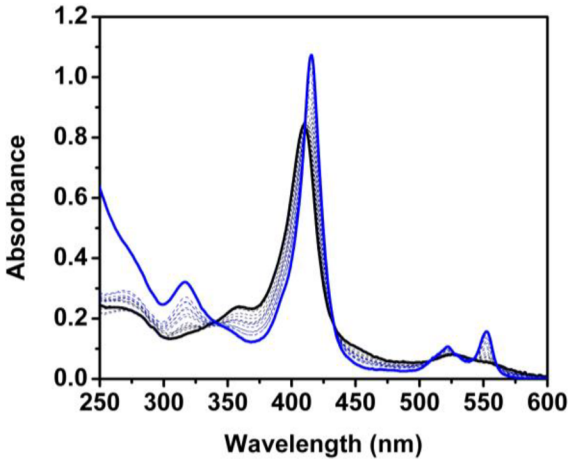

Figure 6. Reduction of cyt c_{550} by DSD-Fdm: UV−vis monitored titration of reduced 300 μM DSD-Fdm to a solution of 7 μM air-oxidized cyt c_{550} in 100 mM Tris, pH 7.5.

that full reduction of the heme was achieved at a 0.74:1 molar ratio of DSD-Fdm/cyt c_{550} (Figure S8, Supporting Information). This stoichiometry is reminiscent of the one-electron reduction processes typically mediated by natural bis-[4Fe-4S] cluster ferredoxins and is consistent with the EPR spin quantification results, because incomplete reduction of the clusters would result in deviation of the ideal 0.5:1 molar ratio for a two electron-carrying ferredoxin that mediates one electron reductions.[25,26,35,36] Together with the similarity in redox potential, these results show that artificial proteins can interface effectively with natural ones to support redox reactivity.

De novo designed redox proteins have been proposed as functional parts of energy harvesting devices.[37−41] To investigate whether holo DSD-Fdm could be used for this application, we investigated the interaction of a porphyrin photosensitizer with the oxidized cluster using laser flash photolysis. Solutions of zinc 5,10,15,20-tetrakis(4-diethyl 2-benzylmalonate) porphyrin (Zn-P, ca. 15 μM; Figure S1, Supporting Information) in deoxygenated buffer were excited at a Q-band (560 nm), and the triplet state lifetimes were probed via the transient absorption at 450 nm. We observed that samples containing either Zn-P only or Zn-P and apo DSD-Fdm had similar triplet lifetimes, ca. 1400 μs, while in the presence of holo DSD-Fdm, the triplet lifetime of Zn-P was significantly shorter, ca. 100 μs (Figure 7). This quenching by a factor of ca. 14 signals electronic interactions between the zinc porphyrin and the iron−sulfur clusters. No signal for oxidized zinc porphyrin was detected at 650 nm.

The Zn-P triplet excited state quenching could occur via three mechanisms: triplet−triplet energy transfer, enhanced intersystem crossing (ISC), or photoinduced electron transfer. Photoinduced electron transfer is exergonic by only about 70 meV, based on the reduction potential for the cluster given above (−0.479 V vs SHE), the first oxidation potential of zinc tetraphenylporphyrin (1.04 V vs SHE), and the energy of the zinc tetraphenylporphyrin triplet state (1.59 eV).[42] Although no porphyrin radical cation was detected, photoinduced electron transfer cannot be completely ruled out because no porphyrin radical cation absorption would be detected if charge

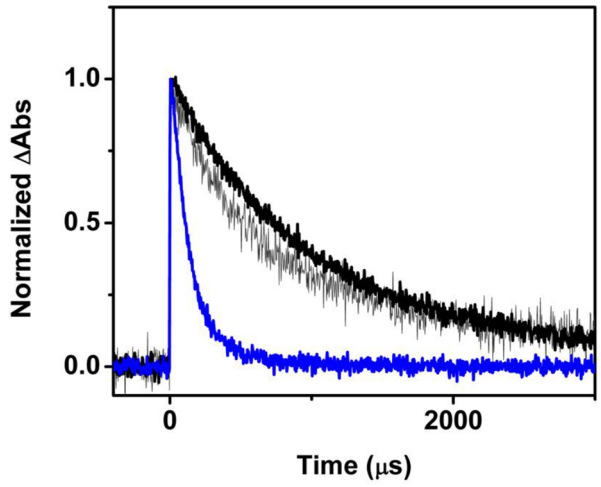

Figure 7. Normalized transient absorption kinetics of Zn-P alone (gray), with apo protein (black), or with holo protein (blue) solutions. The porphyrin was excited at the 560 nm Q-band and probed at 450 nm.

recombination were substantially more rapid than charge separation. Although the available data do not allow us to assign a mechanism for the quenching, all these possibilities require electronic interaction between the porphyrin and the cluster, which necessitates separations of only a few angstroms. Thus, the results show that external reagents can approach the clusters within the peptide closely enough for interesting and potentially useful energy and electron transfer interactions.

CONCLUSIONS

In summary, we designed a protein, DSD-Fdm, in which two [4Fe-4S] clusters are within 12 Å of one another, a distance biologically relevant for effective electron transfer. Both apo and holo DSD-Fdm fold into stable dimers with high helical content. Cofactor binding imparts a significant amount of stability toward chemical denaturation, as often seen in designed metalloproteins.[43,44] The redox potential of DSD-Fdm, −0.479 V vs SHE for the $[4Fe\text{-}4S]^{2+/1+}$ couple, is within the range typical of low-potential ferredoxins. We showed that DSD-Fdm can interface functionally with natural redox proteins by demonstrating stoichiometric electron transfer from reduced DSD-Fdm to oxidized cytochrome *c*. Further, we demonstrated that DSD-Fdm can interact electronically with a photoexcited dye. Compared with their natural counterparts, de novo designed proteins can be specifically tailored in terms of their redox potentials, stability, catalytic properties, protein−protein interactions, and small molecule binding depending on the application desired.[45−55]

The results presented here support the use of de novo designed proteins as redox modules in various applications, ranging from components of artificial redox pathways in synthetic biology to parts of light-driven devices.

ASSOCIATED CONTENT

Supporting Information

NMR and MALDI-TOF spectra of Zn-P and DSD-Fdm, gel filtration chromatograms, ultracentrifugation data, CD spectra, temperature dependence of EPR signal, and UV−vis monitored stoichiometry of cyt *c* reduction. This material is available free of charge via the Internet at http://pubs.acs.org.

dx.doi.org/10.1021/ja510621e | J. Am. Chem. Soc. 2014, 136, 17343−17349

AUTHOR INFORMATION

Corresponding Author

gghirlanda@asu.edu

Present Address

[⊥]A.R.: Department of Biochemistry, Molecular Engineering and Sciences, University of Washington, Seattle, Washington 98195, USA.

Author Contributions

[§]A.R. and D.J.S. contributed equally.

Notes

The authors declare no competing financial interest.

ACKNOWLEDGMENTS

The authors acknowledge Dr. Michael Vaughn for generously providing Cyt c_{550} protein. This work was supported by the Center for Bio-Inspired Solar Fuel Production, an Energy Frontier Research Center funded by the U.S. Department of Energy, Office of Science, Office of Basic Energy Sciences under Award Number DE-SC0001016.

REFERENCES

(1) Han, G. W.; Yang, X. L.; McMullan, D.; Chong, Y. E.; Krishna, S. S.; Rife, C. L.; Weekes, D.; Brittain, S. M.; Abdubek, P.; Ambing, E.; Astakhova, T.; Axelrod, H. L.; Carlton, D.; Caruthers, J.; Chiu, H. J.; Clayton, T.; Duan, L.; Feuerhelm, J.; Grant, J. C.; Grzechnik, S. K.; Jaroszewski, L.; Jin, K. K.; Klock, H. E.; Knuth, M. W.; Kumar, A.; Marciano, D.; Miller, M. D.; Morse, A. T.; Nigoghossian, E.; Okach, L.; Paulsen, J.; Reyes, R.; van den Bedem, H.; White, A.; Wolf, G.; Xu, Q.; Hodgson, K. O.; Wooley, J.; Deacon, A. M.; Godzik, A.; Lesley, S. A.; Elsliger, M. A.; Schimmel, P.; Wilson, I. A. *Acta Crystallogr.* **2010**, *F66*, 1326.

(2) Lill, R. *Nature* **2009**, *460*, 831.

(3) Beinert, H. *Science* **1997**, *277*, 653.

(4) Meyer, J. *J. Biol. Inorg. Chem.* **2008**, *13*, 157.

(5) Stephens, P. J.; Jollie, D. R.; Warshel, A. *Chem. Rev.* **1996**, *96*, 2491.

(6) Durrant, J. D.; de Oliveira, C. A. F.; McCammon, J. A. *J. Mol. Graphics Modell.* **2011**, *29*, 773.

(7) Antonkine, M. L.; Maes, E. M.; Czernuszewicz, R. S.; Breitenstein, C.; Bill, E.; Falzone, C. J.; Balasubramanian, R.; Lubner, C.; Bryant, D. A.; Golbeck, J. H. *Biochim. Biophys. Acta* **2007**, *1767*, 712.

(8) Fontecilla-Camps, J. C.; Volbeda, A.; Cavazza, C.; Nicolet, Y. *Chem. Rev.* **2007**, *107*, 4273.

(9) Johnson, D. C.; Dean, D. R.; Smith, A. D.; Johnson, M. K. *Annu. Rev. Biochem.* **2005**, *74*, 247.

(10) Sweeney, W. V.; Rabinowitz, J. C. *Annu. Rev. Biochem.* **1980**, *49*, 139.

(11) Vignais, P. M.; Billoud, B.; Meyer, J. *FEMS Microbiol. Rev.* **2001**, *25*, 455.

(12) Jin, Z.; Heinnickel, M.; Krebs, C.; Shen, G.; Golbeck, J. H.; Bryant, D. A. *J. Biol. Chem.* **2008**, *283*, 28426.

(13) Dubini, A.; Mus, F.; Seibert, M.; Grossman, A. R.; Posewitz, M. C. *J. Biol. Chem.* **2009**, *284*, 7201.

(14) Mulder, D. W.; Shepard, E. M.; Meuser, J. E.; Joshi, N.; King, P. W.; Posewitz, M. C.; Broderick, J. B.; Peters, J. W. *Structure* **2011**, *19*, 1038.

(15) Peters, J. W.; Lanzilotta, W. N.; Lemon, B. J.; Seefeldt, L. C. *Science* **1998**, *282*, 1853.

(16) Jordan, P.; Fromme, P.; Witt, H. T.; Klukas, O.; Saenger, W.; Krauß, N. *Nature* **2001**, *411*, 909.

(17) Scott, M. P.; Biggins, J. *Protein Sci.* **1997**, *6*, 340.

(18) Antonkine, M. L.; Koay, M. S.; Epel, B.; Breitenstein, C.; Gopta, O.; Gärtner, W.; Bill, E.; Lubitz, W. *Biochim. Biophys. Acta* **2009**, *1787*, 995.

(19) Kennedy, M. L.; Gibney, B. R. *J. Am. Chem. Soc.* **2002**, *124*, 6826.

(20) Grzyb, J.; Xu, F.; Weiner, L.; Reijerse, E. J.; Lubitz, W.; Nanda, V.; Noy, D. *Biochim. Biophys. Acta* **2010**, *1797*, 406.

(21) Grzyb, J.; Xu, F.; Nanda, V.; Luczkowska, R.; Reijerse, E.; Lubitz, W.; Noy, D. *Biochim. Biophys. Acta* **2012**, *1817*, 1256.

(22) Coldren, C. D.; Hellinga, H. W.; Caradonna, J. P. *Proc. Natl. Acad. Sci. U.S.A.* **1997**, *94*, 6635.

(23) Laplaza, C. E.; Holm, R. H. *J. Am. Chem. Soc.* **2001**, *123*, 10255.

(24) Gibney, B. R.; Mulholland, S. E.; Rabanal, F.; Dutton, P. L. *Proc. Natl. Acad. Sci. U.S.A.* **1996**, *93*, 15041.

(25) Roy, A.; Sarrou, I.; Vaughn, M. D.; Astashkin, A. V.; Ghirlanda, G. *Biochemistry* **2013**, *52*, 7586.

(26) Ogihara, N. L.; Ghirlanda, G.; Bryson, J. W.; Gingery, M.; DeGrado, W. F.; Eisenberg, D. *Proc. Natl. Acad. Sci. U.S.A.* **2001**, *98*, 1404.

(27) Mathews, R.; Charlton, S.; Sands, R. H.; Palmer, G. *J. Biol. Chem.* **1974**, *249*, 4326.

(28) Carter, P. *Anal. Biochem.* **1971**, *40*, 450.

(29) Sherman, B. D.; Pillai, S.; Kodis, G.; Bergkamp, J.; Mallouk, T. E.; Gust, D.; Moore, T. A.; Moore, A. L. *Can. J. Chem.* **2011**, *89*, 152.

(30) Torres, R. A.; Lovell, T.; Noodleman, L.; Case, D. A. *J. Am. Chem. Soc.* **2003**, *125*, 1923.

(31) Loewe, R. S.; Ambroise, A.; Muthukumaran, K.; Padmaja, K.; Lysenko, A. B.; Mathur, G.; Li, Q.; Bocian, D. F.; Misra, V.; Lindsey, J. S. *J. Org. Chem.* **2004**, *69*, 1453.

(32) Bencini, A.; Gatteschi, D. *Electron Paramagnetic Resonance of Exchange Coupled Systems*; Springer: Berlin, 2011.

(33) Guldi, D. M.; Zilbermann, I.; Anderson, G.; Li, A.; Balbinot, D.; Jux, N.; Hatzimarinaki, M.; Hirsch, A.; Pra to, M. *Chem. Commun.* **2004**, 726.

(34) Smith, E. T.; Feinberg, B. A. *J. Biol. Chem.* **1990**, *265*, 14371.

(35) Eisenstein, K. K.; Wang, J. H. *J. Biol. Chem.* **1969**, *244*, 1720.

(36) Kyritsis, P.; Hatzfeld, O. M.; Link, T. A.; Moulis, J. M. *J. Biol. Chem.* **1998**, *273*, 15404.

(37) Kathan-Galipeau, K.; Nanayakkara, S.; O'Brian, P. A.; Nikiforov, M.; Discher, B. M.; Bonnell, D. A. *ACS Nano* **2011**, *5*, 4835.

(38) Topoglidis, E.; Discher, B. M.; Moser, C. C.; Dutton, P. L.; Durrant, J. R. *ChemBioChem* **2003**, *4*, 1332.

(39) Lichtenstein, B. R.; Farid, T. A.; Kodali, G.; Solomon, L. A.; Anderson, J. L.; Sheehan, M. M.; Ennist, N. M.; Fry, B. A.; Chobot, S. E.; Bialas, C.; Mancini, J. A.; Armstrong, C. T.; Zhao, Z.; Esipova, T. V.; Snell, D.; Vinogradov, S. A.; Discher, B. M.; Moser, C. C.; Dutton, P. L. *Biochem. Soc. Trans.* **2012**, *40*, 561.

(40) McAllister, K. A.; Zou, H.; Cochran, F. V.; Bender, G. M.; Senes, A.; Fry, H. C.; Nanda, V.; Keenan, P. A.; Lear, J. D.; Saven, J. G.; Therien, M. J.; Blasie, J. K.; DeGrado, W. F. *J. Am. Chem. Soc.* **2008**, *130*, 11921.

(41) Strzalka, J.; Xu, T.; Tronin, A.; Wu, S. P.; Miloradovic, I.; Kuzmenko, I.; Gog, T.; Therien, M. J.; Blasie, J. K. *Nano Lett.* **2006**, *6*, 2395.

(42) Harriman, A. *J. Chem. Soc., Faraday Trans. 1* **1980**, *76*, 1978.

(43) Zastrow, M. L.; Peacock, A. F. A.; Stuckey, J. A.; Pecoraro, V. L. *Nat. Chem.* **2012**, *4*, 118.

(44) Zastrow, M. L.; Pecoraro, V. L. *J. Am. Chem. Soc.* **2013**, *135*, 5895.

(45) Dutton, P. L.; Moser, C. C. *Faraday Discuss.* **2011**, *148*, 443.

(46) Ghirlanda, G.; Lear, J. D.; Ogihara, N. L.; Eisenberg, D.; DeGrado, W. F. *J. Mol. Biol.* **2002**, *319*, 243.

(47) Boyle, A. L.; Woolfson, D. N. *Chem. Soc. Rev.* **2011**, *40*, 4295.

(48) Brodin, J. D.; Carr, J. R.; Sontz, P. A.; Tezcan, F. A. *Proc. Natl. Acad. Sci. U.S.A.* **2014**, *111*, 2897.

(49) Brodin, J. D.; Ambroggio, X. I.; Tang, C.; Parent, K. N.; Baker, T. S.; Tezcan, F. A. *Nat. Chem.* **2012**, *4*, 375.

(50) Huard, D. J. E.; Kane, K. M.; Tezcan, F. A. *Nat. Chem. Biol.* **2013**, *9*, 169.

(51) Mills, J. H.; Khare, S. D.; Bolduc, J. M.; Forouhar, F.; Mulligan, V. K.; Lew, S.; Seetharaman, J.; Tong, L.; Stoddard, B. L.; Baker, D. *J. Am. Chem. Soc.* **2013**, *135*, 13393.

(52) King, N. P.; Bale, J. B.; Sheffler, W.; McNamara, D. E.; Gonen, S.; Gonen, T.; Yeates, T. O.; Baker, D. *Nature* **2014**, *510*, 103.
(53) Tinberg, C. E.; Khare, S. D.; Dou, J.; Doyle, L.; Nelson, J. W.; Schena, A.; Jankowski, W.; Kalodimos, C. G.; Johnsson, K.; Stoddard, B. L.; Baker, D. *Nature* **2013**, *501*, 212.
(54) Berwick, M. R.; Lewis, D. J.; Pikramenou, Z.; Jones, A. W.; Cooper, H. J.; Wilkie, J.; Britton, M. M.; Peacock, A. F. A. *J. Am. Chem. Soc.* **2014**, *136*, 1166−1169.
(55) Peacock, A. F. A. *Curr. Opin. Chem. Biol.* **2014**, *17*, 934−939.